Research on Chemical Intermediates
https://doi.org/10.1007/s11164-020-04085-z

Synthesis and characterization of functionalized NaP Zeolite@$CoFe_2O_4$ hybrid materials: a micro–meso-structure catalyst for aldol condensation

Zohreh Mortezaei[1] · Mojgan Zendehdel[1,2] · Mohammad Ali Bodaghifard[1,2]

Received: 16 October 2019 / Accepted: 9 January 2020

Abstract
In this work, magnetic nanocomposite of NaP Zeolite and $CoFe_2O_4$ as magnetic nanoparticles (MNP's) with different ratios were prepared and in the second step functionalized with 2-aminopyridine as a basic group. All samples were characterized by FT-IR, XRD, VSM, FESEM, EDX, TEM, and BET and thermal analyses. The results show that $CoFe_2O_4$ MNP's was dispersed on NaP Zeolite without any significant aggregation with particle size about 30–50 nm. The BET and TEM confirmed the presence of mesoporous phase in the surface of NaP Zeolite/$CoFe_2O_4$ and preparation a micro–meso-structure. The NaP Zeolite/$CoFe_2O_4$ and NaP Zeolite/$CoFe_2O_4$/Am-Py were used as acid–base catalysts for aldol condensation of cyclohexanone with benzaldehyde, and furfural with acetone which produce curcumin and biofuel intermediates, respectively, in solvent-free condition. The effect of different factors such as the percent of $CoFe_2O_4$ MNP's, catalyst amount, solvent, time and temperature was investigated. The catalyst was easily separated with an external magnet and reused four times without significant change in the yield. These catalysts have various advantages including high loading capacity, low leaching for $CoFe_2O_4$ MNP's and simple and efficient recovery procedure which can be used under mild and ecofriendly condition.

Keywords Zeolite/$CoFe_2O_4$ · Functionalization · Aminopyridine · Micro–meso-structure · Aldol condensation

✉ Mojgan Zendehdel
m-zendehdel@araku.ac.ir; mojganzendehdel@yahoo.com

[1] Department of Chemistry, Faculty of Science, Arak University, Arak 38156-8-8349, Iran

[2] Institute of Nanosciences and Nanotechnology, Arak University, Arak, Iran

Published online: 21 January 2020

Introduction

Organic transformations are very important, and their products are used in many areas such as biology, pharmacology and industry [1–3]. Based on the principles of green chemistry, designing novel and high efficient catalysts is important for organic synthesis. Then, the preparation of recoverable heterogeneous catalysts has been a long goal in catalyst research. Recent studies have shown that hybrid materials such as inorganic–inorganic [4, 5] or inorganic–organic [5, 6] material were widely used as some heterogeneous catalysts for organic reactions. Also, during the last decade significant efforts have been devoted to the development of catalysts with both acid and base sites guaranteeing a large number of highly active and fully accessible catalytic sites for organic reaction [7].

Increasing attention has recently been paid to the use of magnetic nanoparticles (MNPs) as support [8, 9]. One of the important magnetic materials with spinel structure is cobalt ferrite ($CoFe_2O_4$) which is due to high efficiency, low leaching of cobalt and ferromagnetic nature, and easy separation from aqueous solution usually is promising as a catalyst for organic synthesis [10, 11]. It is well known that magnetic particles synthesized by different methods are usually agglomerated and their specific area and catalytic efficiency decreased [12, 13]. An effective method to prevent the agglomeration is dispersing of particles on a stable support. The porous materials, such as zeolites with good acidity, high surface areas and well-defined structures, can be used as a support for different materials. However, introducing $CoFe_2O_4$ MNP's to zeolite may decrease the catalytic activity due to diffusion limitation of microporous materials, but increase the acidity. There are many reports which show the surface of MNP's functionalized by different materials such as organic, organometallic and acidic groups which are useful for many organic reactions [14, 15].

Although the surface of the MNP's and zeolite with free silanol groups (Si–OH) are suitable agents for functionalization [16, 17], immobilizing of amine groups to Zeolite/$CoFe_2O_4$ has not yet been reported.

Aldol condensation is one of well-known organic syntheses to form the C–C bond which was done in the presence of either basic or acidic catalysts such as zeolite [18], MgO–ZrO_2 [19], MFI [20], $MnFe_2O_4$/g–C_3N_4 [21]. The aldol products are found in many natural compounds such as antibiotics, bioactive and biomass-derived materials. For example, some works proposed a method to obtaining high length of carbon chain diesel fuels; the key step of it is the aldol condensation between furfural and acetone [22–24]. Although many of these recyclable catalysts are environmentally friendly, acidic sites can be catalyzed side reactions and produce coke and deactivate the catalyst [25]. Also, in the basic media the product of aldol condensation depends on the condition of preparation [26].

The goal of the present study is to design and develop a new hybrid catalyst which can be used as heterogeneous acid–base catalyst for aldol condensation reaction. For that purpose, the NaP Zeolite/$CoFe_2O_4$ nanocomposites were prepared and functionalized with 2-aminopyridine; then the prepared catalysts (NaP Zeolite/$CoFe_2O_4$/Am-Py) were used for two sets of aldol condensation reaction.

In this approach, the structure of catalyst and its efficiency in organic reactions were considered.

Experimental

Materials and methods

All materials and solvents were purchased from Aldrich and Merck. Fourier Transform Infrared analysis was recorded by a Galaxy series FT-IR 5000 spectrometer. The patterns of X-ray diffraction were recorded by an X-Ray diffractometer (Philips 1840) with Cr-Kα radiation. The chemical compositions of the samples were determined by elemental analysis (Vario E1III)) and energy-dispersive X-ray spectroscopy (Oxford X-max). The thermogravimetric analysis (TGA) and differential thermal analysis (DTA) were performed using a Diamond Pyris TM, TG/DT 6300 from 30 to 600 °C at a heating rate of 10 °C/min under argon flow. Scanning electron microscope (SEM) images of the samples were obtained using a Zeiss Sigma-VP FESEM instrument. Brunauer-Emmett-Teller apparatus (SIBATA, App, 1100-SA with adsorption of nitrogen at 76.34 K) was used. VSM analysis was carried out by AGFM operation and EM900/ZISS. A Bruker Avance 300 MHz spectrometer was used for ^{1}HNMR spectra to characterization of organic compound. The high-resolution transmission electron microscopy (HRTEM) images of samples were obtained using a Zeiss Libra (200 kV). The products were analyzed by an Agilent 7890A GC unit equipped with a flame ionization (FID) detector using a HP-5 capillary column (30 m/0.32 ID/0.25 m) and the gas chromatography–mass spectrometry (GC–MS) analysis.

Synthesis of $CoFe_2O_4$ nanoparticles

The $CoFe_2O_4$ nanoparticle was synthesized according to a previously reported procedure [27]. 1.19 g of $CoCl_2{\cdot}6H_2O$ and 2.70 g of $FeCl_3{\cdot}6H_2O$ were added in 50 mL deionized water. Then, a solution of NaOH (3 mol/L) was added to it and stirred at 80 °C for 1 h under N_2 atmosphere. The mixture of reaction was cooled to room temperature, and the solid product was separated by an external magnet and washed with ethanol and then dried under vacuum at 50 °C for 24 h.

Preparation of NaP Zeolite/$CoFe_2O_4$ nanocomposites

Different amounts of $CoFe_2O_4$ (0.125, 0.250, 0.375, 0.500 g) were added to a fresh gel of zeolite with the molar composition of 320 H_2O:16 NaOH:1 $Al(OH)_3$:15 SiO_2 which agitated for 5 days and stirred for 5 h and finally placed in an autoclave at 100 °C for 24 h. After cooling the reaction mixture to room temperature, the solid material (NaP Zeolite/$CoFe_2O_4$ nanocomposite) was filtered and washed with water until pH = 9 and dried in air [28].

Preparation of NaP Zeolite/$CoFe_2O_4$/Am-Py nanocomposites

In the first step, 1 mmol of 3-chloropropyltrimethoxysilane (3-ClPTMS) was reacted with 1.2 mmol 2-aminopyridine in 5 mL dry toluene at 90 °C under nitrogen atmosphere for 30 h. The resulting material (3-APPTMS) was added to 0.5 g of NaP Zeolite/$CoFe_2O_4$ composite in 10 mL dry toluene refluxing for 24 h under nitrogen atmosphere. Finally, the solid material, NaP Zeolite/$CoFe_2O_4$/Am-Py, was filtered, washed by chloroform, ethanol and water, respectively, and dried at 100 ˚C for 24 h and then was characterized by FT-IR, XRD, TEM, SEM, EDS, TGA, BET and VSM techniques [29].

Consideration of the catalytic activity (aldol condensation)

To consider the catalytic activity of prepared hybrid material, two reactions were selected which are explained as follow: (a) at a 10 ml flask, 1 mmol cyclohexanone was added to 2 mmol of 4-X-benzaldehyde derivatives and then different amounts of catalysts (NaP Zeolite/$CoFe_2O_4$ and NaP Zeolite/$CoFe_2O_4$/Am-Py) were added to the mixture. The reaction mixtures were magnetically stirred at room temperature and under nitrogen atmosphere. The reactions were monitored by TLC. After completion, the catalyst was separated with a magnet and the solid residue, recrystallized with ethanol to give the pure product.

(b) Aldol condensation reaction was carried out in 10-mL flask. Different amounts of catalyst were added to a mixture of 0.43 ml of furfural and a certain amount of acetone (the mole ratios of furfural/acetone are 1:10, 1:5, 1:2). Thereafter, the mixture was refluxed at 100 °C under stirring for different times. After reaction completion as monitored by TLC, the flask was quickly cooled down to room temperature using an ice bath. Then, the resulting solid product was filtered and recrystallized with ethanol for several times to remove the remained organics and was identified based on the standard reference compounds and GC–MS analyses.

Results and discussion

The alkylaminopyridine-decorated NaP Zeolite/$CoFe_2O_4$ nanocomposite (NaP Zeolite/$CoFe_2O_4$/Am-Py) as a hybrid acid–base heterogeneous catalyst was prepared sequentially depicted in Scheme1. $CoFe_2O_4$ nanoparticles were prepared by co-precipitation method (Fe^{+3} and Co^{+2} ions in basic solution). The different amounts of

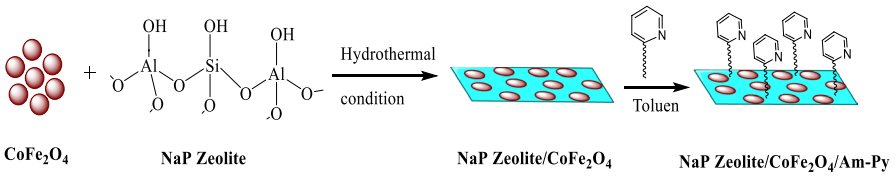

Scheme1 The sequential synthesis of NaP Zeolite/$CoFe_2O_4$/Am-Py hybrid material

$CoFe_2O_4$ (0.125, 0.250, 0.375, 0.500 g) were added to a fresh gel of zeolite to obtain the NaP Zeolite/$CoFe_2O_4$ nanocomposites. The obtained nanocomposite was functionalized by (3-Aminopyridinopropyl) triethoxysilane (3-APPTS) to produce aminopyridine-decorated magnetic hybrid nanomaterial (NaP Zeolite/$CoFe_2O_4$/Am-Py).

FT-IR spectra

The FT-IR spectroscopic data for pure $CoFe_2O_4$ nanoparticles and NaP Zeolite/$CoFe_2O_4$ nanocomposite with different amounts of $CoFe_2O_4$, before and after functionalization by alkylaminopyridine, are summarized in Table 1.

Literature reviews show the bands at 417 cm^{-1} and 592 cm^{-1} that involves the stretching vibration of Fe–O (Fe^{+3}–O^{-2}) on the octahedral and tetrahedral sites, [30] after creating NaP Zeolite/$CoFe_2O_4$ nanocomposite has been hidden due to the broad bands related to zeolite structure. The appearance a peak at 1012 cm^{-1} attribute to the asymmetric stretching of Al–O–Si chain and two bonds about 745 and 437 cm^{-1} related to symmetric stretching and bending frequency of Al–O–Si, respectively was confirmed the presence of NaP zeolite in the nanocomposite structure [31]. Several bonds about 1422, 2958 cm^{-1} and 1731, 3450 cm^{-1} relating to C–N, C–H and N–H groups, related to alkylaminopyridine moiety can be observed. The peaks at 3434 and 1625 cm^{-1} are assigned to O–H stretching.

XRD analysis

The XRD patterns for $CoFe_2O_4$, NaP Zeolite/$CoFe_2O_4$ and NaP Zeolite/$CoFe_2O_4$/Am-Py are shown in Fig. 1A and B. It can be observed seven characteristic peaks at the 2θ values of 18.6, 31.6, 36.0, 45.6, 54.1, 56.9 and 66.5, which corresponded to (1 1 1), (2 2 0), (3 1 1), (4 0 0), (4 2 2), (5 1 1) and (4 4 0) reflections, respectively [Fig. 1A (a)] and confirm the cubic reverse spinel phase of $CoFe_2O_4$ (JCPDS 221086) [32].

After introducing different amounts of $CoFe_2O_4$ to zeolite structure, all the composites show similar characteristic peaks ($2\theta = 12.48°$, 17.92°, 21.79°, 28.1° and 33.4°) Fig. 1A (b–e) [33] related to NaP Zeolite beside the $CoFe_2O_4$ reflections. Also, the results show that after functionalization of NaP Zeolite/$CoFe_2O_4$ nanocomposite by alkylaminopyridine [Fig. 1B (f–i)], due to interaction of 3-ClPTMS with zeolite, small amounts of amorphous phase were observed [12]. It seems the modification of NaP Zeolite/$CoFe_2O_4$ nanocomposite surface did not significantly affect the crystallinity of $CoFe_2O_4$ phase but decreasing the intensity suggests that some of these MNPs are incorporated to the zeolite pores which is in agreement to other reports [34, 35].

The crystallite size of these as-synthesized $CoFe_2O_4$ in the composite with different percent was estimated from the full width at half maximum (FWHM) of strongest diffraction peak $2\theta = 54.1$ using the Scherrer's equation [29], $D = 0.9\ \lambda/(\beta \text{ Cos } 2\theta)$ where D is the crystallite size, λ is the wavelength of Cr-Kα radiation, β is FWHM, and θ is the diffraction angle of the strongest characteristic

Table 1 The FT-IR data for $CoFe_2O_4$ and NaP Zeolite/$CoFe_2O_4$ before and after functionalization with aminopyridine moiety

Sample	Internal vibrations			External vibrations		C–N	N–H bend	C–H aliphatic	N–H stretch
	T–O bend	T–O υ_{sym}	T–O υ_{asym}	T–O υ_{sym}	D-R				
$CoFe_2O_4$	–	–	–	–	–	–	–	–	–
NaP Zeolite/$CoFe_2O_4$ (1:1)	437	688	1013	745	607	–	–	–	–
NaP Zeolite/$CoFe_2O_4$ (1:2)	437	686	1012	745	607	–	–	–	–
NaP Zeolite/$CoFe_2O_4$ (1:3)	437	687	1009	745	608	–	–	–	–
NaP Zeolite/$CoFe_2O_4$ (1:4)	438	684	1012	745	607	–	–	–	–
NaP Zeolite/$CoFe_2O_4$/Am-Py (1:1)	438	692	1016	745	607	1421	1737	2959	3454
NaP Zeolite/$CoFe_2O_4$/Am-Py (1:2)	438	692	1013	745	607	1423	1735	2958	3450
NaP Zeolite/$CoFe_2O_4$/Am-Py (1:3)	437	689	1012	745	607	1428	1738	2958	3456
NaP Zeolite/$CoFe_2O_4$/Am-Py (1:4)	437	694	1013	745	606	1422	1736	2957	3445

T–O, T = Al, Si

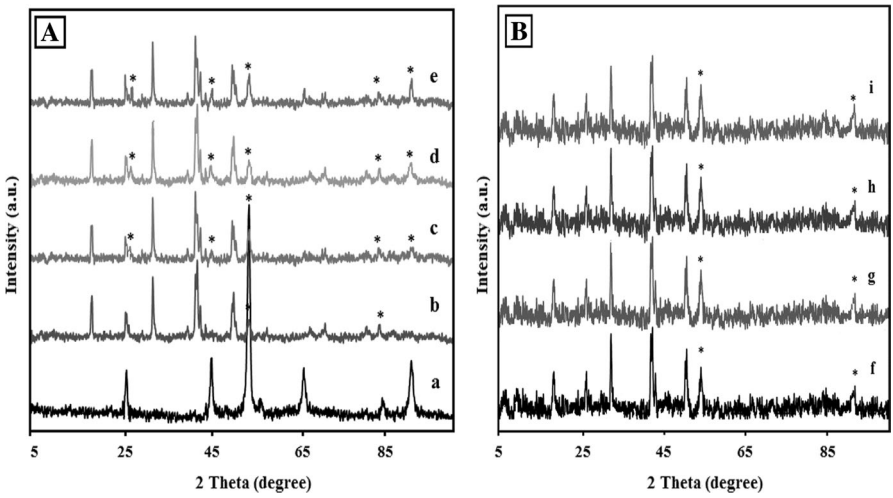

Fig. 1 The XRD pattern, Part **A**: for $CoFe_2O_4$ (a), NaP Zeolite/$CoFe_2O_4$(1:1) (b), NaP Zeolite/$CoFe_2O_4$(1:2) (c), NaP Zeolite/$CoFe_2O_4$(1:3) (d), NaP Zeolite/$CoFe_2O_4$ (1:4) (e), Part **B**: for NaP Zeolite/$CoFe_2O_4$/Am-Py (1:1) (f), NaP Zeolite/$CoFe_2O_4$/Am-Py (1:2) (g), NaP Zeolite/$CoFe_2O_4$/Am-Py (1:3) (h), NaP Zeolite/$CoFe_2O_4$/Am-Py (1:4) (i)

peak. The data show that the crystallite size of MNPs was increased from 50 nm to the range of 60–100 nm when introduced to composite which may be due to agglomeration.

Figure 2A and B shows the low-angle XRD region for NaP Zeolite/$CoFe_2O_4$ and NaP Zeolite/$CoFe_2O_4$/Am-Py nanocomposite, respectively. The results show the low intensity of Bragg X-ray reflections about $2\theta = 1.8°$, 3.9° and 4.4° related to the lines (100), (110) and (200) that can be indexed as a hexagonal mesoporous material [36], indicating that the obtained mesoporous are not completely ordered. Also the intensity of reflections was decreased after functionalization by amine group which may be due to the lack of structural order in mesoscale material [37] and creating amorphous phase.

The nitrogen adsorption/desorption

The nitrogen adsorption/desorption isotherm and the pore size distribution of NaP Zeolite/$CoFe_2O_4$ with 1:2 and 1:4 percent before and after functionalization are described in Fig. 3A and B. A sudden increase in the N_2 isotherm [Fig. 3A (a, b)] at the low-pressure region about $P/P0 < 0.1$ confirms the existence of microporous phase [38]. Also, the presence of hysteresis loop at pressure $P/P0$ of 0.5–1, that is the type-IV isotherm, indicates the mesoporous phase [39]. The results show that after functionalization of NaP Zeolite/$CoFe_2O_4$ with amine [Fig. 3B (a, b)] the microporous phase decreased and also a rapid increase at high-pressure region about $P/P0 > 0.9$ suggests the existence of macroporous

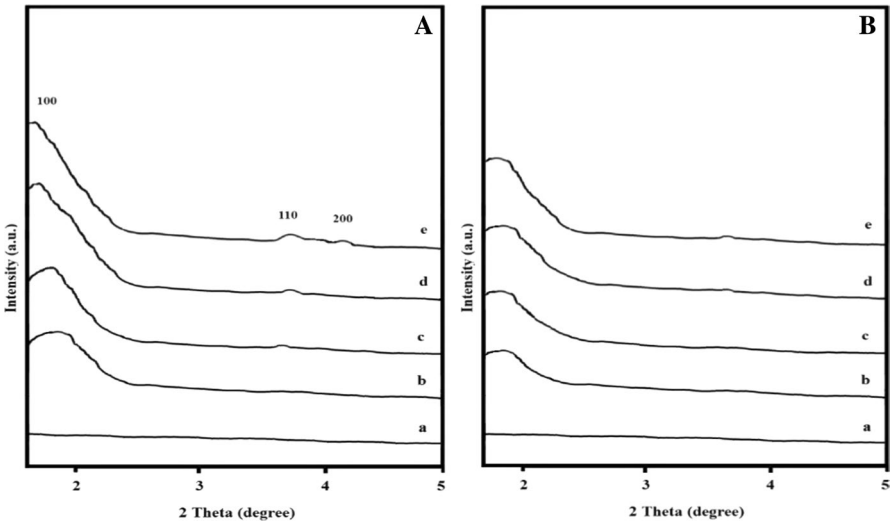

Fig. 2 The XRD in low angle range, Part **A**: NaP Zeolite (a), NaP Zeolite/$CoFe_2O_4$ (1:1) (b), NaP Zeolite/$CoFe_2O_4$ (1:2) (c), NaP Zeolite/$CoFe_2O_4$ (1:3) (d), NaP Zeolite/$CoFe_2O_4$ (1:4) (e) Part **B**: for Nap (a) and NaP Zeolite/$CoFe_2O_4$/Am-Py (1:1) (b), NaP Zeolite/$CoFe_2O_4$/Am-Py (1:2) (c), NaP Zeolite/$CoFe_2O_4$/Am-Py (1:3) (d), NaP Zeolite/$CoFe_2O_4$/Am-Py (1:4) (e)

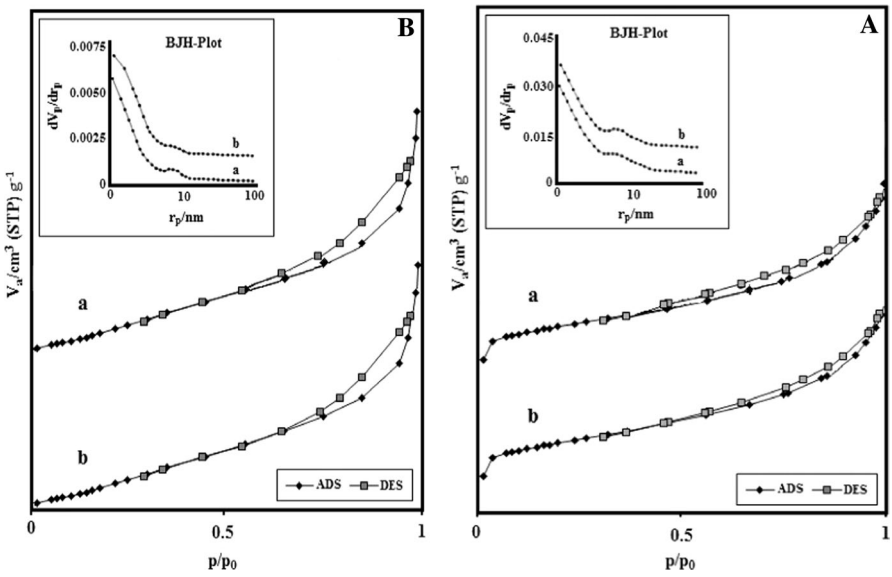

Fig. 3 Nitrogen adsorption/desorption isotherms and BJH Plot of part **A**: NaP Zeolite/$CoFe_2O_4$ (1:2) (a), NaP Zeolite/$CoFe_2O_4$ (1:4) (b) and part **B**: NaP Zeolite/$CoFe_2O_4$/Am-Py (1:2) (a), NaP Zeolite/$CoFe_2O_4$/Am-Py (1:4) (b)

phase [40]. The decrease in the pore volume and pore area after functionalization of zeolite by alkylaminopyridine can be attributed to the introducing some of amine groups into the NaP Zeolite/$CoFe_2O_4$ nanocomposite and also creating new mesophase on the surface of zeolite.

Also the results in Table 2 (calculated using BET, BJH, and t-Plot methods) show that after introducing $CoFe_2O_4$ in the zeolite framework, the surface area for NaP Zeolite (45 m^2/g) increased due to increasing the mesophase which confirms the presence of hierarchical structure for zeolite. The pore size distribution in Fig. 3A and B for all cases shows two ranges of particle size 1–8 nm corresponding to mesoporous phase and greater than 8 nm related to microporous phase and confirms this conclusion [12, 41].

SEM, TEM, EDX and elemental analysis

The SEM images of the $CoFe_2O_4$ nanoparticles and NaP Zeolite/$CoFe_2O_4$ nanocomposite with 1:2 and 1:4 ratios before and after functionalization are shown in Fig. 4a–h. Figure 4a and b shows quasi-spherical morphology for $CoFe_2O_4$ nanoparticles and exhibits a rough surface and average diameter of about 40 nm. After introducing magnetic nanoparticles into zeolite, wool ball-like [42] morphology was observed for 1:2 (c, d) and 1:4 (e, f) ratios and also the presence of spherical MNPs which have been shown by yellow circles. For NaP Zeolite/$CoFe_2O_4$ with higher percent of MNPs, small agglomeration can be observed (Fig. 4f) which confirms the particle size increasing in Scherrer's equation. The images for functionalized NaP Zeolite/$CoFe_2O_4$ with 1:2 and 1:4 ratios in Fig. 4g and h, respectively, show that the morphology of NaP Zeolite is not changed, but the percent of amorphous phase increased. Figure 5a–d shows that the Co and Fe uniformly were dispersed over the zeolite support (NaP Zeolite/$CoFe_2O_4$) with 1:2 ratios.

The size and shape of NaP Zeolite/$CoFe_2O_4$ nanocomposite (1:2 and 1:4) are observed in Fig. 6a–d using high-resolution TEM. The images show that the quasi-spherical $CoFe_2O_4$ with average diameter about 38 nm completely dispersed on zeolite in the 1:2 ratios without any agglomeration, but with increasing the percent of $CoFe_2O_4$, in some parts agglomeration can be seen. Also closer images of TEM (Fig. 6b, d) show the intracrystalline worm-like mesoporous phase without any order in the surface of samples which these results are in agreement with other literature reports [43]. Also, after functionalization of NaP Zeolite/$CoFe_2O_4$ nanocomposite with aminopyridine moiety in two different ratios (NaP Zeolite/$CoFe_2O_4$/Am-Py), mesoporous phase was decreased (Fig. 6e, f) which confirms the small amounts of amorphous phase which observed in XRD and decreasing S_{meso} in BET.

The chemical composition of materials was considered by EDX and elemental analysis (C, H, N) (Table 3). The results for the C/N (about 2.8) and Si/Al ~ 2.3) and Fe/Co (about 2) in all samples are very close to real ratios and confirm the presence of NaP Zeolite, $CoFe_2O_4$ and alkylaminopyridine in the nanocomposite.

Table 2 The BET data of NaP Zeolite/$CoFe_2O_4$ nanocomposite and NaP Zeolite/$CoFe_2O_4$/Am-Py hybrid material

Sample	S^{a}_{BET} (m^2/g)	S^{b}_{micro} (m^2/g)	S_{meso} (m^2/g)	V^{c}_{t} (cm^3/g)	V^{b}_{micro} (cm^3/g)	V^{d}_{meso} (cm^3/g)	d_{BJH} (nm)
NaP Zeolite/$CoFe_2O_4$ (1:1)	151.30	41.32	109.98	0.2	0.09	0.11	1.29
NaP Zeolite/$CoFe_2O_4$ (1:2)	149.25	40.02	109.23	0.2	0.08	0.12	1.29
NaP Zeolite/$CoFe_2O_4$ (1:3)	145.02	44.85	100.17	0.18	0.07	0.11	1.29
NaP Zeolite/$CoFe_2O_4$ (1:4)	140.42	30.59	109.83	0.17	0.05	0.13	1.19
NaP Zeolite/$CoFe_2O_4$/Am-Py (1:1)	50.25	30.07	20.18	0.08	0.04	0.04	1.29
NaP Zeolite/$CoFe_2O_4$/Am-Py (1:2)	44.37	28.40	15.97	0.07	0.04	0.03	1.29
NaP Zeolite/$CoFe_2O_4$/Am-Py (1:3)	39.05	18.37	20.68	0.05	0.02	0.03	1.29
NaP Zeolite/$CoFe_2O_4$/Am-Py (1:4)	30.87	10.49	20.38	0.04	0.01	0.03	1.29

[a]Calculated by the BET method

[b]Calculated by the t-plot method

[c]Obtained at a relative pressure of 0.99

[d]Calculated by the BJH method

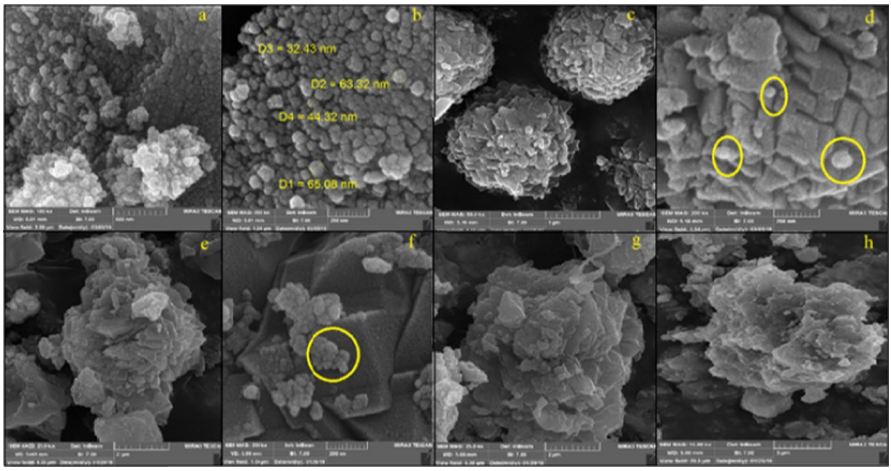

Fig. 4 The SEM images of the $CoFe_2O_4$ (**a**, **b**) nanoparticles and NaP Zeolite/$CoFe_2O_4$ with 1:2 and 1:4 ratios before (**c**, **d**) (**e**, **f**) and after functionalize with amine (**g**, **h**)

Thermogravimetric analysis

The TGA and DTG curves of NaP/$CoFe_2O_4$ samples before and after functionalization at different ratios (1:2 and 1:4) are shown in Fig. 7A and B, respectively. The TGA curve as shown in Fig. 7A is divided into three steps. The first weight loss in 30–200 °C is attributed to the removal of physisorbed and chemisorbed water. The second step, for NaP Zeolite/$CoFe_2O_4$ accompanied with endothermic peaks in DTG, can be corresponded to the dehydration of the hydroxyl groups inside the micro- and meso-phases [44, 45] and also changing the structure of $CoFe_2O_4$. In the case of NaP Zeolite/$CoFe_2O_4$/Am-Py hybrid material, the percent of weight loss in the second step increased about 4% due to thermal decomposition of the organic moiety and also in the DTA curves two endothermic peaks can be seen; the first peak about 200–320 °C confirmed the presence of alkylaminopyridine in the structure [45, 46]. The last steps might be related to some transformations of phase of gismondine-like structures and $CoFe_2O_4$, respectively [31].

The measurement of magnetic properties (VSM)

The magnetic properties of $CoFe_2O_4$, NaP Zeolite/$CoFe_2O_4$, and NaP Zeolite/$CoFe_2O_4$/Am-Py samples were examined using a vibrating sample magnetometer (VSM) from −20 000 to 20 000 Oe at room temperature (Fig. 8 and Table 4). The results in Table 4 show that the saturation magnetizations of the $CoFe_2O_4$ MNPs are about 67.58% of the $CoFe_2O_4$ bulk materials value. $CoFe_2O_4$ is well-known hard magnetic material due to its high saturation magnetization about 80 emu/g and high coercivity 5400 Oe; these values depended on particle size and synthesis methods [47].

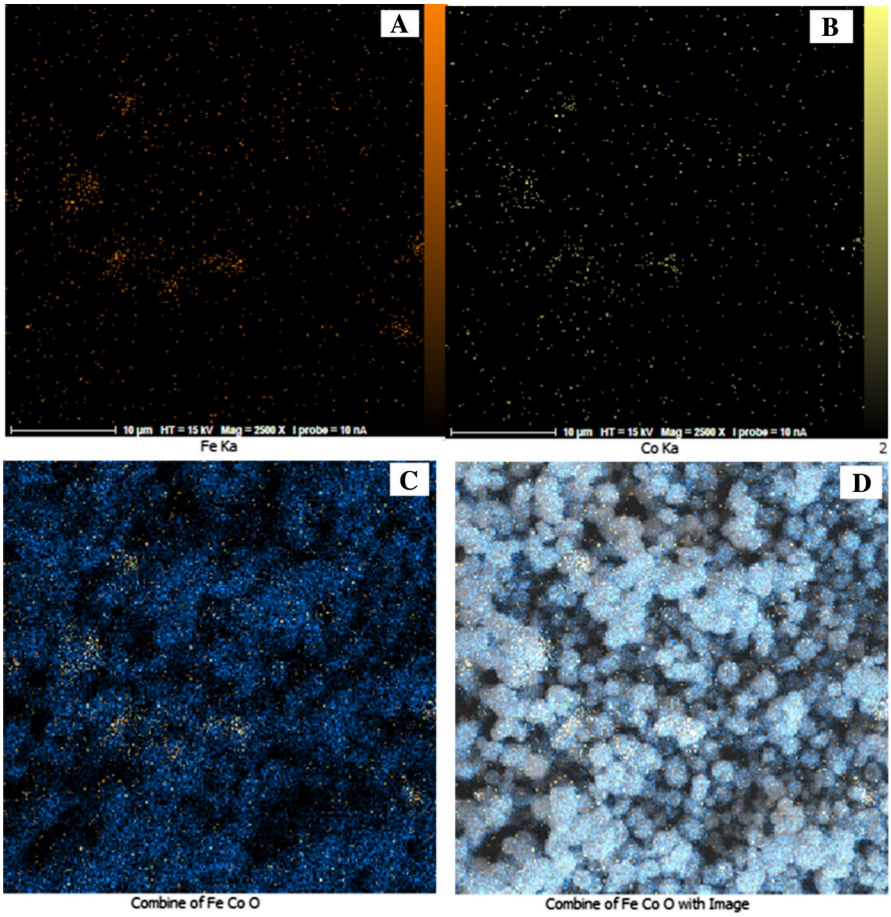

Fig. 5 Elemental mapping of NaP Zeolite/$CoFe_2O_4$ nanocomposite with 1:2 ratios (**a**–**c**) and 1:4 ratio (**d**)

MNPs are introduced to NaP Zeolite with different ratio and also after functionalize amine decreased. These results may be due to (1) increasing size of MNps after introducing zeolite (2) high interaction between $CoFe_2O_4$ nanoparticles and zeolite (3) and covering of nanoparticles by zeolite and alkylaminopyridine [48, 49]. Also, the shape of slope in the magnetic hysteresis loops confirmed that all materials exhibit non-negligible coercivity (Hc) and very low remanence (Mr) at room temperature, indicating superparamagnetic behavior for all samples [50, 51]. Also, same as other works with introducing $CoFe_2O_4$ to NaP Zeolite and functionalization by alkylaminopyridine, the both saturation magnetization and coercivity of the composites are lower than its bulk values.

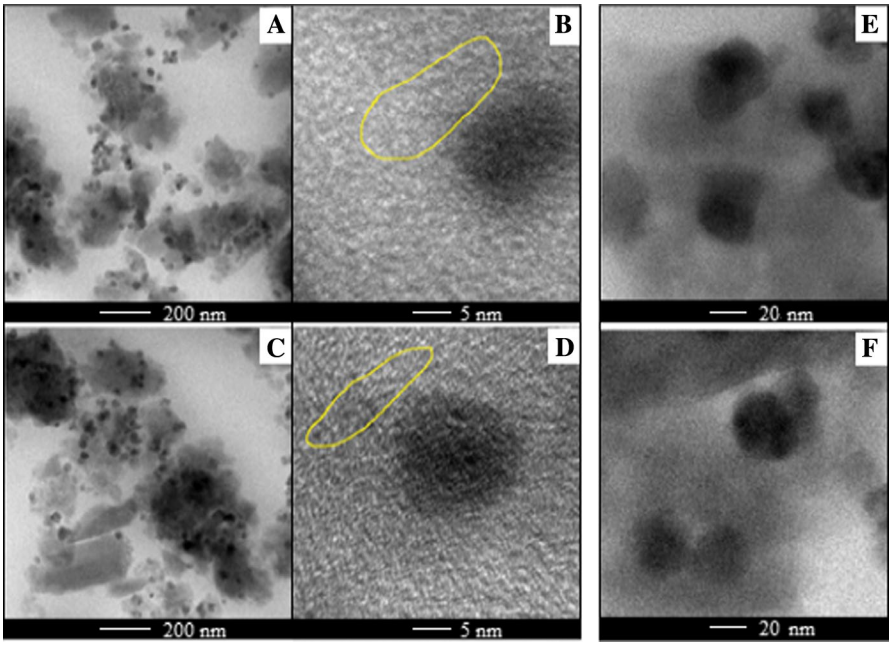

Fig. 6 The TEM images for NaP Zeolite/$CoFe_2O_4$ (1:2) (**a**, **b**), NaP Zeolite/$CoFe_2O_4$ (1:4) (**c**, **d**), NaP Zeolite/$CoFe_2O_4$/Am-Py (1:2) (**e**) and NaP Zeolite/$CoFe_2O_4$/Am-Py (1:4) (**f**)

Table 3 The elemental analysis of NaP Zeolite/$CoFe_2O_4$ nanocomposite and NaP Zeolite/$CoFe_2O_4$/Am-Py hybrid material

Sample	% O	C/N	Si/Al	Fe/Co
$CoFe_2O_4$	48.97	–	–	1.94
NaP Zeolite/$CoFe_2O_4$ (1:2)	40.32	–	2.26	1.97
NaP Zeolite/$CoFe_2O_4$ (1:4)	41.89	–	2.36	2.00
NaP Zeolite/$CoFe_2O_4$/Am-Py (1:2)	41.03	2.79	2.27	1.84
NaP Zeolite/$CoFe_2O_4$/Am-Py (1:4)	40.30	2.74	2.31	1.93

Catalytic activity

We know the aldol condensation as one of the most important reactions to forming C–C bonds, and the condensation of cycloalkanones with aldehydes and ketones has been widely used for preparation of many compounds such as antibiotics and bioactive materials [52–54]. The preparation of these compounds such as curcumin which have excellent anti angiogenic effects is important for future animal model studies. Then, this work focused on the preparation of these compounds by easy, economical and mild conditions.

The aldol condensation results of cyclohexanone with benzaldehyde derivatives with different ratio of catalysts (NaP Zeolite/$CoFe_2O_4$ and NaP Zeolite/$CoFe_2O_4$/Am-Py) are shown in Table 5. The results indicate that the pure $CoFe_2O_4$ and NaP

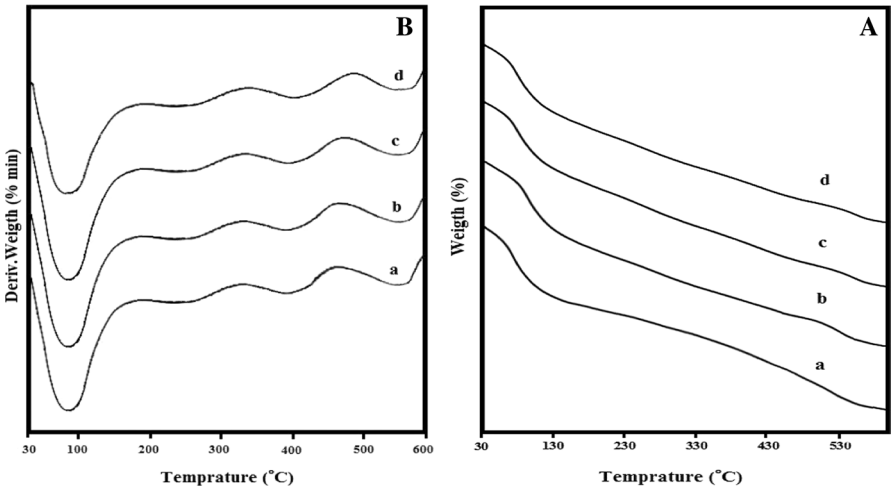

Fig. 7 TGA curves (part **A**) and DTG curves (part **B**) of NaP Zeolite/$CoFe_2O_4$/Am-Py (1:1) (a), NaP Zeolite/$CoFe_2O_4$/Am-Py (1:2) (b), NaP Zeolite/$CoFe_2O_4$/Am-Py (1:3) (c), NaP Zeolite/$CoFe_2O_4$/Am-Py (1:4) (d)

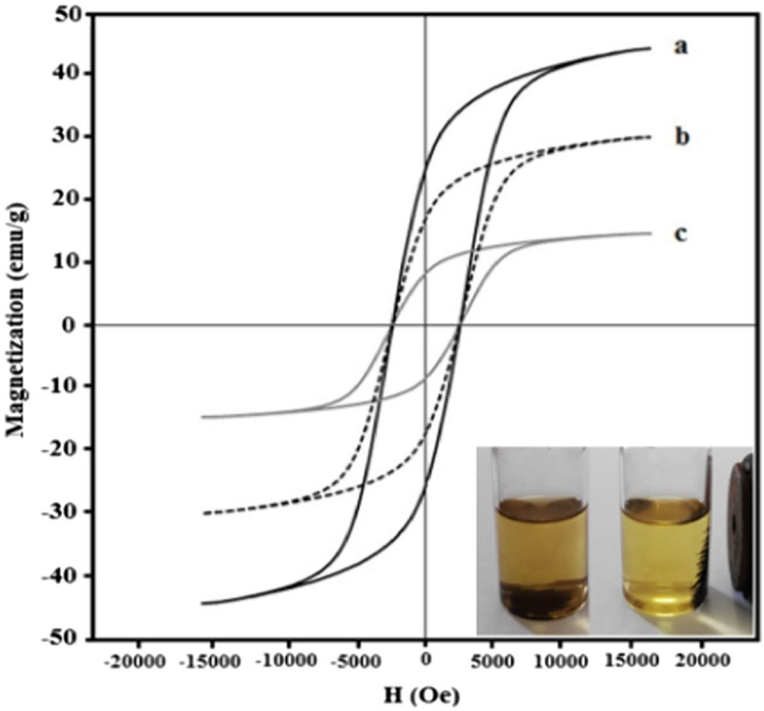

Fig. 8 Magnetic hysteresis curves of $CoFe_2O_4$ (a), NaP Zeolite/$CoFe_2O_4$ (1:4) (b) and NaP Zeolite/$CoFe_2O_4$/Am-Py (1:4) powders (c)

Table 4 The magnetic properties of $CoFe_2O_4$ nanoparticles, NaP Zeolite/$CoFe_2O_4$ nanocomposite, and NaP Zeolite/$CoFe_2O_4$/Am-Py hybrid nanomaterial

Sample	Ms (emu/g)	Mr (emu/g)	Hc (Oe)
$CoFe_2O_4$	46.40	26.30	2500
NaP Zeolite/$CoFe_2O_4$ (1:2)	24.72	15.30	2500
NaP Zeolite/$CoFe_2O_4$ (1:4)	31.36	18.92	2500
NaP Zeolite/$CoFe_2O_4$/Am-Py (1:2)	12.97	7.05	2500
NaP Zeolite/$CoFe_2O_4$/Am-Py (1:4)	16.81	9.49	2500

Table 5 Aldol condensation of cyclohexanone with benzaldehyde derivatives over catalysts. Reaction conditions: cyclohexanone (1 mmol), 4-X-benzaldehyde (X = H, Cl) (2 mmol), reaction temperature (room temperature) and reaction time (16 h), Catalyst amount (20 mg)

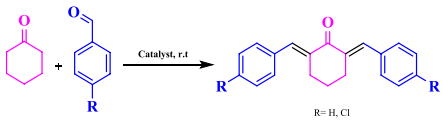

Entry	Catalyst	Solvent	Aldehyde	Yield (%)
1	NaP Zeolite	Solvent-free	Benzaldehyde	38
2	NaP Zeolite	Solvent-free	4-Chlorobenzaldehyde	39
3	$CoFe_2O_4$	Solvent-free	Benzaldehyde	42
4	$CoFe_2O_4$	Solvent-free	4-Chlorobenzaldehyde	43
5	NaP Zeolite/$CoFe_2O_4$ (1:1)	Solvent-free	Benzaldehyde	45
6	NaP Zeolite/$CoFe_2O_4$ (1:1)	Solvent-free	4-Chlorobenzaldehyde	43
7	NaP Zeolite/$CoFe_2O_4$ (1:2)	Solvent-free	Benzaldehyde	49
8	NaP Zeolite/$CoFe_2O_4$ (1:2)	Solvent-free	4-Chlorobenzaldehyde	55
9	NaP Zeolite/$CoFe_2O_4$ (1:3)	Solvent-free	Benzaldehyde	60
10	NaP Zeolite/$CoFe_2O_4$ (1:3)	Solvent-free	4-Chlorobenzaldehyde	68
11	NaP Zeolite/$CoFe_2O_4$ (1:4)	Solvent-free	Benzaldehyde	73
12	NaP Zeolite/$CoFe_2O_4$ (1:4)	Solvent-free	4-Chlorobenzaldehyde	79
13	NaP Zeolite/$CoFe_2O_4$ (1:4)	CH_2Cl_2	Benzaldehyde	70
14	NaP Zeolite/$CoFe_2O_4$ (1:4)	CH_2Cl_2	4-Chlorobenzaldehyde	76
15	NaP Zeolite/$CoFe_2O_4$ (1:4)	EtOH	Benzaldehyde	68
16	NaP Zeolite/$CoFe_2O_4$ (1:4)	EtOH	4-Chlorobenzaldehyde	69
17	NaP Zeolite/$CoFe_2O_4$/Am-Py (1:1)	Solvent-free	Benzaldehyde	62
18	NaP Zeolite/$CoFe_2O_4$/Am-Py (1:1)	Solvent-free	4-Chlorobenzaldehyde	64
19	NaP Zeolite/$CoFe_2O_4$/Am-Py (1:2)	Solvent-free	Benzaldehyde	78
20	NaP Zeolite/$CoFe_2O_4$/Am-Py (1:2)	Solvent-free	4-Chlorobenzaldehyde	77
21	NaP Zeolite/$CoFe_2O_4$/Am-Py (1:3)	Solvent-free	Benzaldehyde	85
22	NaP Zeolite/$CoFe_2O_4$/Am-Py (1:3)	Solvent-free	4-Chlorobenzaldehyde	87
23	NaP Zeolite/$CoFe_2O_4$/Am-Py (1:4)	Solvent-free	Benzaldehyde	92
24	NaP Zeolite/$CoFe_2O_4$/Am-Py (1:4)	Solvent-free	4-Chlorobenzaldehyde	96

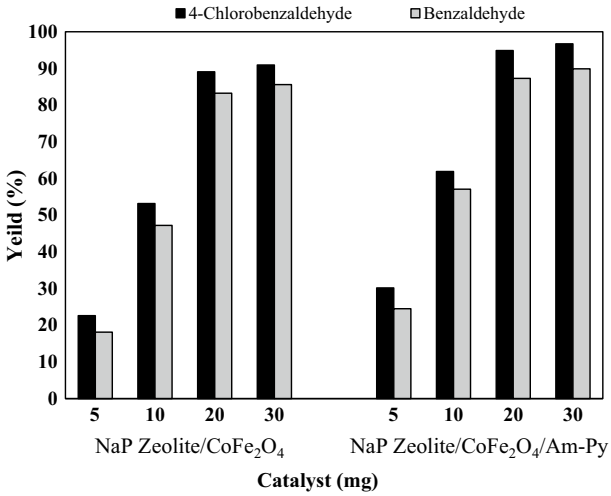

Fig. 9 The effect of amounts for NaP Zeolite/$CoFe_2O_4$ and NaP Zeolite/$CoFe_2O_4$/Am-Py catalyst (ratio 1:4) in aldol condensation reaction at room temperature and 16 h

Zeolite produced relatively low yields (entries 1–4) and with decreasing the ratio of NaP Zeolite/$CoFe_2O_4$, the yield was increased (entries 5–12 and 17–24). The presence of aminopyridine moieties has a good effect on the yield (entries 17–24). It seems, with introducing the basic amine groups on NaP Zeolite/$CoFe_2O_4$ nanocomposite, an acid–base catalyst was created which is useful for aldol condensation. One of the effective factors in the progress of reaction is the amount of catalyst (Fig. 9) because the result shows that for lower catalyst amount, the lower yield was obtained which confirms the higher amounts of acid and base site in the cavities and surface of catalyst is useful for the reaction. Furthermore, the reaction had no significant change in the yield of reactions for nonpolar solvent (entries 13 and 14), but with using of polar solvents such as ethanol, the yield of reaction was reduced (entries 15 and 16) which may be due to strong interaction between solvent (through oxygen atoms) and acid–base sites of the catalyst [55]. So, the prepared hybrid catalysts show high efficiency at room temperature and easy work-up in which the separation techniques are not necessary to get the pure compounds. To consider the effect of temperature and time on the yield of the reaction, aldol condensation was studied at 50 °C and 12 h time. The result showed that the yield of the reaction for NaP Zeolite/$CoFe_2O_4$ and NaP Zeolite/$CoFe_2O_4$/Am-Py had small increase (about 2–3%) with temperature rising and also the yield was decreased about 10% with reduction in reaction time, which confirm that the reaction follows from Arrhenius equation [55]. The proposed mechanism is shown in Scheme 2.

Selected spectroscopic data

2,6-Di(benzylidene)cyclohexan-1-one m.p. 117 °C; FT-IR (KBr, cm^{-1}): 1583 (C=C), 1677 (C=O), 2982 (C–H Aliphatic), 3055 (C–H Aromatic); ^{1}H-NMR

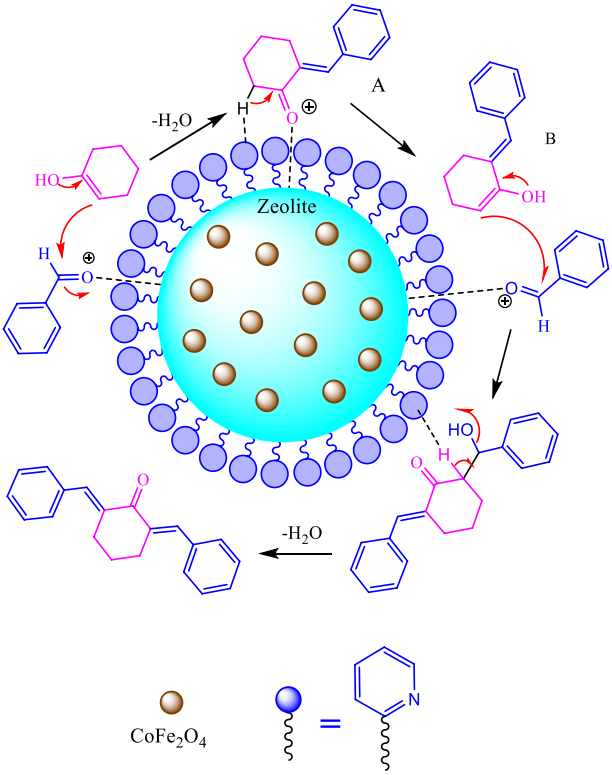

Scheme 2 The plausible mechanism for the Crossed-Aldol condensation in the presence of NaP Zeolite/$CoFe_2O_4$/Am-Py (1:4) as a heterogeneous catalyst

(400 MHz, $CDCl_3$, δppm): 1.79 (m, 2H, $H_{Aliph.}$), 2.93 (m, 4H, $H_{Aliph.}$), 7.33-7.46 (m, 10H, $H_{Arom.}$), 7.80 (s, 2H, $H_{Olefin.}$).

2,6-Bis(4-chlorobenzylidene)cyclohexan-1-one m.p. 147–148 °C; FT-IR (KBr, cm^{-1}): 1600 (C=C), 1660 (C=O), 2914 (C–H Aliphatic), 2938 (C–H Aromatic); ^{1}H-NMR (400 MHz, $CDCl_3$, δppm): 1.80 (m, 2H, $H_{Aliph.}$), 2.88 (m, 4H, $H_{Aliph.}$), 7.38 (m, 8H, $H_{Arom.}$), 7.72 (s, 2H, $H_{Olefin.}$).

Biomass is a new organic source for energy industry. Some aldol condensation reactions such as condensation of furfural and acetone produce an intermediate which can be used for preparation of short chain biomass derivatives [25]. Literature survey revealed that aldol condensation between furfural and acetone was formed FAcOH (4-(2-furyl)-4-hydroxy-butan-2-one) as a primary condensation product; this intermediate compound subsequently dehydrated into the aldol product FAc (Table 6) and then it can be reacted with another furfural molecule to produce the aldol dimer product F_2Ac. Firstly, NaP Zeolite and $CoFe_2O_4$ nanoparticles were used as catalysts for aldol reaction (entries 1–2), but small conversion was found at

Table 6 Aldol condensation of furfural with acetone over catalysts. Reaction conditions: 20 mg catalyst, Furfural (0.01 mol), Acetone (0.1 mol), temperature (100 °C) and reaction time (2 h)

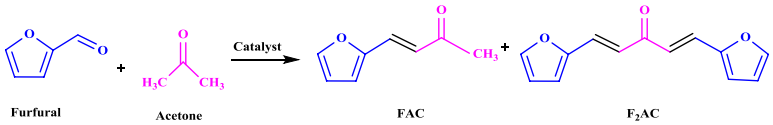

Selectivity (%)	Furfural conversion (%)	Catalyst	Entry	Selectivity (%)
			FAc	F_2Ac
1	NaP Zeolite	36.5	71.1	15.3
2	$CoFe_2O_4$	55.9	78.3	12.3
3	NaP Zeolite/$CoFe_2O_4$ (1:1)	67.9	81.7	11.1
4	NaP Zeolite/$CoFe_2O_4$ (1:2)	80.4	84.3	9.7
5	NaP Zeolite/$CoFe_2O_4$ (1:3)	89.8	87.8	7.7
6	NaP Zeolite/$CoFe_2O_4$ (1:4)	96.1	89.8	6.1
7	NaP Zeolite/$CoFe_2O_4$/Am-Py (1:1)	69.2	83.9	11.6
8	NaP Zeolite/$CoFe_2O_4$/Am-Py (1:2)	83.4	85.7	10.0
9	NaP Zeolite/$CoFe_2O_4$/Am-Py (1:3)	92.3	88.6	8.2
10	NaP Zeolite/$CoFe_2O_4$/Am-Py (1:4)	97.9	92.3	6.7

reaction conditions. The furfural conversion was increased with decreasing the ratio of NaP Zeolite/$CoFe_2O_4$ for pure and functionalized catalyst (entries 3–6 and 7–10). During the reaction, F_2Ac as a product was detected, but the maximum selectivity in preparation of F_2Ac (11.61%) was achieved at maximum furfural conversion (Table 6, entry 7). It seems the size of cavities in the micro-/meso-catalyst (NaP Zeolite/$CoFe_2O_4$ and NaP Zeolite/$CoFe_2O_4$/Am-Py) is suitable for the production of FAc, because previous studies showed that the size of aldol adduct, F_2Ac, is up to 1.4 nm and highly non-spherical [24]. According to the BJH, micropores distributions for NaP Zeolite/$CoFe_2O_4$ and NaP Zeolite/$CoFe_2O_4$/Am-Py (Fig. 3) are less than 1.4 nm; therefore, the catalyst can be prevented from the second condensation steps between furfural and FAc to form F_2Ac [19]. Although, with introducing amino pyridine to the NaP Zeolite/$CoFe_2O_4$, the selectivity for preparation of F_2Ac was increased which confirms the effect of basic sites for construction of F_2Ac, functional groups may also prevent the formation of the large sized molecule F_2AC, so small yield increase in F_2Ac was observed [25, 56].

To consider the effect of molar ratio between furfural and acetone, three ratios (1:10, 1:5 and 1:2) were used (Fig. 10). The results show that the conversion of furfural increased about 7% and the selectivity of F_2Ac decreased 2% with decreasing the ratio of furfural/acetone. L. Faba and co-workers reported that the separation of proton from acetone and forming the carbon anion intermediate is the rate determining step for the aldol condensation of furfural and acetone, then with decreasing the acetone in the reaction mixture, the interaction between the catalyst and acetone reduced, and the furfural conversion was decreased [57]. The

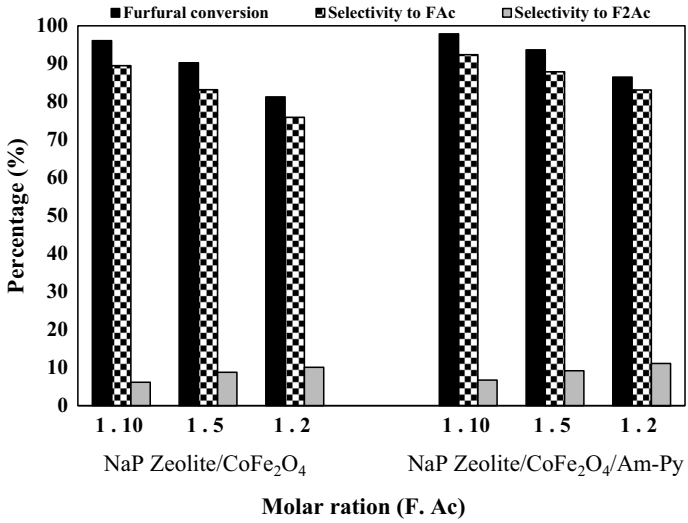

Fig. 10 The effect of molar ratio between furfural and acetone (1:10, 1:5 and 1:2) in aldol condensation with 20 mg catalyst, 2 h reaction time at 100 °C

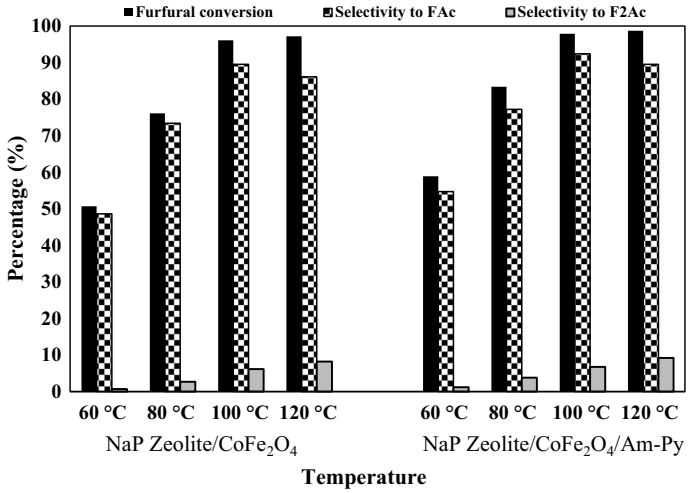

Fig. 11 The effect of temperature on catalytic activity in aldol condensation of furfural and acetone with 2 h and 20 mg catalyst

effect of temperature was investigated on reaction time on (2 h) at $T = 60$, 80, 100 and 120 °C (Fig. 11) which results show that the furfural conversion increased with increasing temperature and selectivity remains at very low changing. These results are in agreement with previous studies that show high furfural conversion, and the selectivity to aldol products in aldol condensation can be achieved by high reaction temperature [18, 58]. Also, the result of GC analysis indicated the

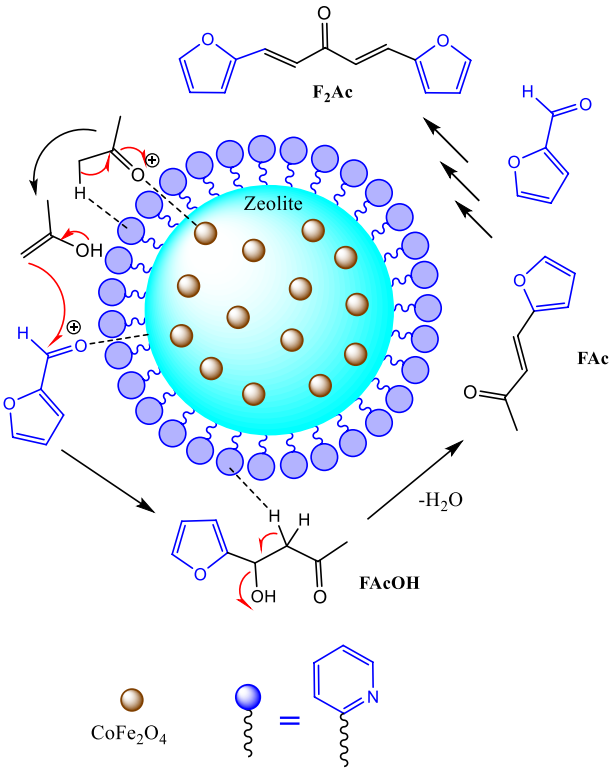

Scheme 3 The proposed mechanism for production of FAc as a biomass derivative in the presence of NaP Zeolite/$CoFe_2O_4$/Am-Py as a shape selective catalyst

presence of FAcOH during the reaction, which confirms the proposed mechanism in Scheme 3.

Also, the catalytic activity comparison of NaP Zeolite/$CoFe_2O_4$/Am-Py(1:4) with other reported heterogeneous catalysts for aldol condensation of furfural and acetone which produce FAc and F_2Ac shows in this work the condition of reaction (amount of catalyst, yields, time and temperature of reaction) is very mild and ecofriendly due to solvent-free condition (Table 7) [18, 25, 59–64].

Recycling ability of the catalyst

The catalytic recycling experiments were also conducted on NaP Zeolite/$CoFe_2O_4$ and NaP Zeolite/$CoFe_2O_4$/Am-Py, and the results are shown in Fig. 12. After first run the catalysts separated with a magnet and solid powder was washed thoroughly with dichloromethane and ethanol and then dried in vacuum condition and used for the next 4 runs. The results show that the yields reduced about 5–7% in each run. It seems this effect is due to lower decreasing in saturation magnetization and coercivity factor

Table 7 Comparison of catalytic activity of NaP Zeolite/$CoFe_2O_4$/Am-Py (1:4) with other reported heterogeneous catalysts

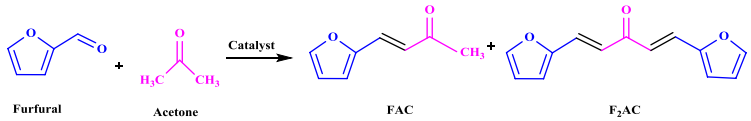

Catalyst (amount of cat. g)	Temp. (°C)	Time (min)	Furfural Conversion (%)	Selectivity (%)		Ref.
				FAC	F_2AC	
MgO-ZrO_2 (0.5)	100	180	70.0	45.0	10.0	[59]
HTC (Mg/Al:3) (2)	100	120	95.0	90.0	–	[60]
MgO/NaY (1.06)	85	480	99.6	42.2	57.1	[61]
Mg-Zr/HSAG (0.5)	50	1440	96.5	90.0	–	[62]
Mg-Zr Oxide (0.5)	50	1440	98.4	14.7	61.5	[62]
HBEA-25 (2)	100	120	38.5	79.5	3.7	[18]
Fe-BTC (1)	100	240	26.2	71.0	20.0	[63]
BEA (1)	100	240	29.0	83.0	5.5	[63]
K-IE-Y-2.5 (2)	100	120	8.3	96.4	1.5	[25]
K-IMP-Y-15 (2)	100	44.1	35.0	35.0	17.0	[25]
K-PVA-10% (0.25)	100	120	96.4	90.3	4.0	[64]
NaP Zeolite/$CoFe_2O_4$/Am-Py(1:4) (0.02)	100	120	97.9	92.3	6.75	–

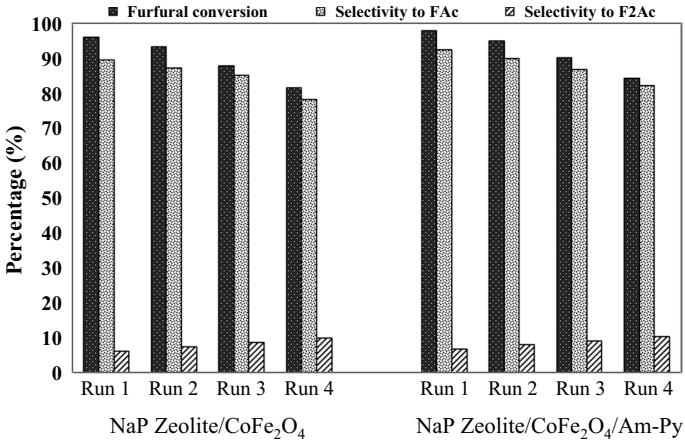

Fig. 12 The catalytic recycling results of NaP Zeolite/$CoFe_2O_4$ and NaP Zeolite/$CoFe_2O_4$/Am-Py (ratio 1:4)

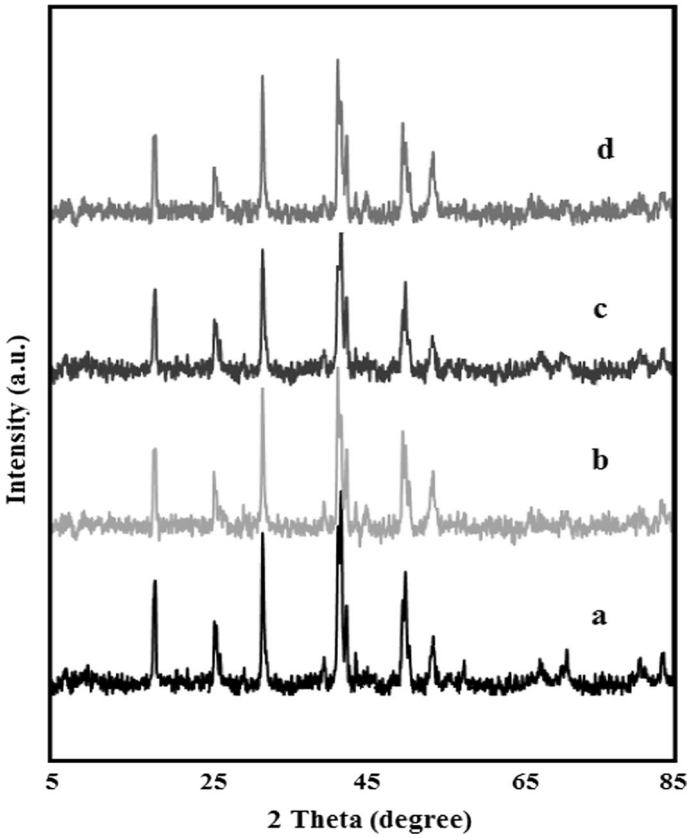

Fig. 13 The XRD patterns of NaP Zeolite/$CoFe_2O_4$ (1:4) as a fresh catalyst (a) and after 4 runs using as a catalyst for aldol condensation reactions for (b) cyclohexanone with benzaldehyde, (c) cyclohexanone with 4-Cl-benzaldehyde and (d) furfural and acetone

respect to other works which is an important parameter for reuse during the organic reaction [65, 66].

The result shows that the yield of the reactions reduces about 5–7% in each run (Fig. 13). Figure 13a–d shows the XRD patterns of fresh and reused catalyst [NaP Zeolite/$CoFe_2O_4$ (1:4)] in aldol condensation reactions. Figure 13b, c is related to the reaction of cyclohexanone with benzaldehyde and with 4-Cl-benzaldehyde, respectively. Also, Fig. 13d shows the XRD pattern of reused catalyst [NaP Zeolite/$CoFe_2O_4$ (1:4)] in aldol condensation of furfural and acetone. The obtained XRD patterns show that the structure of catalyst after final runs has not changed and is the same as fresh catalyst.

Conclusion

The $CoFe_2O_4$ nanoparticles, with uniformly distributed 40 nm size, with different ratios introduced to gel of zeolite and under hydrothermal condition a micro–meso-structures of zeolite, were prepared. Then, the NaP Zeolite/$CoFe_2O_4$ nanostructure functionalized with 2-aminopyridine tags as a basic organic moiety. The structure of hybrid nanostructure (NaP Zeolite/$CoFe_2O_4$/Am-Py) was confirmed by FT-IR, XRD, BET, VSM, TG, SEM and TEM techniques. In the second step, the catalytic properties of prepared materials were investigated by two sets of aldol condensation reaction as follow:

1. In crossed-aldol condensation of cyclohexanone with aromatic aldehydes, the products yields were higher than pure zeolite and $CoFe_2O_4$ and also with introducing aminopyridine to inorganic support; the yield of reaction was increased.
2. The condensation of furfural with acetone in the presence of prepared micro–meso-nanomaterial produced FAc in high yield while F_2Ac was a side product. These results confirm that the size of micro–meso-structure cavities is appropriate for small molecules. Besides, the conversion and shape selectivity is affected with the change in the molar ratio of furfural: acetone and reaction temperature.

   So, it seems both acidic and basic sites are effective on aldol condensation reactions. The prepared hybrid catalyst was easily separated and reused several times without significant loss of its activity. The presented catalysts can be used at mild conditions and have potential for industrial application as heterogeneous catalysts.

Acknowledgements Thanks to the Iranian Nanotechnology Innovation Council and the Research Council of Arak University and Center of Excellence in the Chemistry Department of Arak University for supporting of this work.

References

1. M.M. Dutta, P. Phukan, Catal. Commun. **109**, 38 (2018)
2. G. Evano, N. Blanchard, M. Toumi, Chem. Rev. **108**, 3054 (2008)
3. F. Monnier, M. Taillefer, Angew. Chem. Int. Ed. **47**, 3096 (2008)
4. P. Zhang, Q. Han, M. Fan, P. Jiang, Appl. Surf. Sci. **317**, 1125 (2014)
5. S. Rostamnia, E. Doustkhah, RSC Adv. **4**, 28238 (2014)
6. M. Zendehdel, F. Zamani, H. Khanmohamadi, Microporous Mesoporous Mater. **225**, 552 (2016)
7. G.A. Ferrero, K. Preuss, A. Marinovic, A.B. Jorge, N. Mansor, D.J.L. Brett, A.B. Fuertes, M. Sevilla, M.M. Titirici, ACS Nano **10**, 5922 (2016)
8. Q. Zhang, X. Yang, J. Guan, ACS Appl. Nano Mater. **2**(8), 4681 (2019)
9. Z. Li, S. Wu, Ch. Yang, Y. Ma, X. Fu, L. Peng, J. Guan, Q. Kan, Mol. Catal. **432**, 267 (2017)
10. Ch. Yi-long, S. Jia-qiang, Z. Yan-feng, Z. Shen-ke, W. Bu-huan, Ch. Zheng, X. Ying-ying, Ch. Min, M. Abbas, Ch. Jian-gang, J. Fuel. Chem. Technol. **45**(9), 1082 (2017)
11. X. Tan, X. Wang, Q. Liu, J. Zhou, P. Zhang, S. Zheng, S. Miao, J. Hydrogen Energy **42**(30), 19001 (2017)
12. Y. Du, W. Ma, P. Liu, B. Zou, J. Ma, J. Hazard. Mater. **308**, 58 (2016)

13. Y. Wang, H. Zhao, M. Li, J. Fan, G. Zhao, Appl. Catal. B **147**, 534 (2014)
14. M.A. Bodaghifard, M. Hamidinasab, N. Ahadi, Curr. Org. Chem. **22**, 234 (2018)
15. G. Bayramoglu, B. Salih, M.Y. Arica, Appl. Biochem. Biotechnol. (2019).
16. C.M. Crudden, M. Sateesh, R. Lewis, J. Am. Chem. Soc. **127**, 10045 (2005)
17. X.S. Zhao, G.Q. Lu, A.K. Whittaker, G.J. Millar, H.Y. Zhu, J. Phys. Chem. B **101**, 6525 (1997)
18. O. Kikhtyanin, V. Kelbichova, D. Vitvarova, M. Kubu, D. Kubicka, Catal. Today **227**, 154 (2014)
19. W. Shen, G.A. Tompsett, K.D. Hammond, R. Xing, F. Dogan, C.P. Grey, W.C. Conner Jr., S.M. Auerbach, G.W. Huber, Appl. Catal. A Gen. **392**, 57 (2011)
20. M.X. Su, W.Z. Li, T.W. Zhang, H.S. Xin, S. Li, W. Fan, L.L. Ma, Catal. Sci. Technol. **7**, 3555 (2017)
21. B. Bhuyan, D.J. Koiri, M. Devi, S.S. Dhar, Mater. Lett. **218**, 99 (2018)
22. G.W. Huber, J.N. Chheda, C.J. Barret, J.A. Dumesic, Science **308**, 1446 (2005)
23. C.J. Barret, J.N. Chheda, G.W. Huber, J.A. Dumesic, Appl. Catal. B Environ. **66**, 111 (2006)
24. P. Kustrowski, D. Sulkowska, L. Chmielarz, A. Rafalska-Lasocha, B. Dudek, R. Dziembaj, Microporous Mesoporous Mater. **78**, 11 (2005)
25. O. Kikhtyanin, Y. Ganjkhanlou, D. Kubicka, R. Bulanek, J. Cejka, Appl. Catal. A **549**, 8 (2018)
26. O. Kikhtyanin, R. Bulanek, K. Frolich, J. Cejka, D. Kubicka, J. Mol. Catal. A Chem. **424**, 358 (2016)
27. X.N. Zhao, HCh. Hu, F.J. Zhang, Z. Zhang, Appl. Catal. A **482**, 258 (2014)
28. M. Zendehdel, M. Ramezani, B. Shoshtari-Yeganeh, G. Cruciani, A. Salmani, Environ. Technol. (2018).
29. M. Esmaeilpour, J. Javidi, F.N. Dodeji, M.M. Abarghoui, J. Mol. Catal. A Chem. **393**, 18 (2014)
30. K.W. Wagner, Ann. Phys. **40**, 818 (1913)
31. D. Chandra, T. Yokoi, T. Tatsumi, A. Bhaumik, Chem. Mater. **19**, 5347 (2007)
32. J.K. Rajput, G. Kaur, Catal. Sci. Technol. **4**, 142 (2014)
33. S. Hansen, U. Hakansson, L. Faelth, Acta Crystallogr. Sect. C Cryst. Struct. Commun. **46**, 1361 (1990)
34. A.H. Alwash, A.Z. Abdullah, N. Ismail, J. Hazard. Mater. **233–234**, 184 (2012)
35. M. Abecassis-Wolfovich, R. Jothiramalingam, M.V. Landau, M. Herskowitz, B. Viswanathan, T.K. Varadarajan, Appl. Catal. B Environ. **59**, 91 (2005)
36. I.I. Ivanova, E.E. Knyazeva, Chem. Soc. Rev. **42**, 3671 (2013)
37. K. Na, M. Choi, R. Ryoo, Microporous Mesoporous Mater. **166**, 3 (2013)
38. J.H. Hou, K. Jiang, R. Wei, M. Tahir, X.G. Wu, M. Shen, X.Z. Wang, C.B. Cao, J. ACS Appl. Mater. Interfaces **9**, 30626 (2017)
39. M. Fu, W. Chen, J. Ding, X. Zhu, Q. Liu, J. Alloys Compd. **782**, 952 (2019)
40. Q. Wang, Q. Cao, X.Y. Wang, B. Jing, H. Kuang, L. Zhou, J. Power Sources **225**, 101 (2013)
41. O. Mazaheri, R.J. Kalbasi, RSC Adv. **5**, 34398 (2015)
42. Z. Huo, X. Xu, Z. Lu, J. Song, M. He, Z. Li, Q. Wang, L. Yan, Microporous Mesoporous Mater. **158**, 137 (2012)
43. J. Jin, Ch. Peng, J. Wang, H. Liu, X. Gao, H. Liu, Ch. Xu, Ind. Eng. Chem. Res. **53**, 3406 (2014)
44. F. Zamani, M. Zendehdel, A. Mobinikhaledi, M. Azarkish, Microporous Mesoporous Mater. **2**, 18 (2015)
45. S. Wang, B. He, R. Tian, Ch. Sun, R. Dai, X. Li, X. Wu, X. An, X. Xie, J. Colloid Interface Sci. **527**, 339 (2018)
46. H. Zhang, Y.F. Fan, Y.H. Huan, M.B. Yue, Microporous Mesoporous Mater. **231**, 178 (2016)
47. D. Giap, R.S. Turtelli, W.C. Nunes, E. Schafler, N. Hanh, R. Grossinger, M. Knobel, J. Non Cryst. Solids **353**, 805 (2007)
48. R. Ianoşn, M. Bosca, R. Lazau, Ceram. Int. **140**, 10223 (2014)
49. B.J. Rani, M. Ravina, B. Saravanakumar, G. Ravi, V. Ganesh, S. Ravichandran, R. Yuvakkumar, Nano Struct. Nano Objects **14**, 84 (2018)
50. R. Tabit, O. Amadine, Y. Essamlali, K. Danoun, A. Rhihil, M. Zahouily, RSC Adv. **8**, 1351 (2018)
51. N. Song, S. Gu, Q. Wu, Ch. Li, J. Zhou, P. Zhang, W. Wang, M. Yue, J. Magn. Magn. Mater. **451**, 793 (2018)
52. K. Manabe, Y. Mori, S. Nagayama, K. Odashima, S. Kobayashi, Inorg. Chim. Acta **296**, 158 (1999)
53. J.M. Fraile, I. Perez, J.A. Mayoral, J. Catal. **252**, 303 (2007)
54. T.P. Robinson, T. Ehlers, R. Hubbard, X. Bai, J.L. Arbiser, D.J. Goldsmith, J.P. Bowen, Bioorg. Med. Chem. Lett. **13**, 115 (2003)
55. S.K. Sharma, P.A. Parikh, R.V. Jasra, J. Mol. Catal. A Chem. **278**, 135 (2007)

56. F. Winter, V. Koot, A.J. Dillen, J.W. Geus, K.P. de Jong, J. Catal. **236**, 91 (2005)
57. L. Faba, E. Diaz, S. Ordonez, Appl. Catal. B Environ. **113–114**, 201 (2012)
58. X.M. Huang, Q. Zhang, T.H. Wang, Q.Y. Liu, L.L. Ma, Q. Zhang, J. Fuel Chem. Technol. **40**, 973 (2012)
59. I. Sadaba, M. Sanchez, O.M. Sanchez, O.R. Mariscal, R. Mariscal, M.L. Granados, M.L. Granados, Appl. Catal. B Environ. **101**(3–4), 638 (2011)
60. L. Hora, V. Kelbichova, O. Kikhtyanin, O. Bortnovskiyb, D. Kubicka, Catal. Today **223**, 138 (2014)
61. X.M. Huang, Q. Zhang, T.J. Wang, Q.Y. Liu, Q. Zhang, J. Fuel Chem. Technol. **40**(8), 973 (2012)
62. L. Faba, E. Daz, S.O. Çez, ChemSusChem **6**, 463 (2013)
63. O. Kikhtyanin, D. Kubicka, J. Cejka, Catal. Today **243**, 158 (2015)
64. T. Zhan, S. Wu, H. Ma, Ch. Yue, Z. Huang, W. Liu, J. Teng, D. Lia, S. Wang, H. Tan, Microporous Mesoporous Mater. **281**, 101 (2019)
65. T.A. Arica, E. Ayas, M.Y. Arica, Microporous Mesoporous Mater. **243**, 164 (2017)
66. G. Bayramoglu, T. Doz, V.C. Ozalp, M.Y. Arica, Food Chem. **15**(221), 1442 (2017)